The Effect of Bridging on Fatigue Crack Growth Behavior in Aramid Patched Aluminum Alloy(APAL)

S. W. Oh*, W. J. Park*, C. W. Hue*, H. K. Yoon and K. B. Lee*****

(Received February 7, 1994)

A new hybrid composite (APAL ; Aramid Patched Aluminum Alloy), consisting of a 2024-T3 aluminum alloy plate sandwiched between two aramid/epoxy laminate (HK 285/RS 1222), was developed. Fatigue crack growth behavior was examined at stress ratios of R=0.2, 0.5 using the aluminum alloy and two kinds of the APAL with different fiber orientation (0°/90°and 45° for crack direction). The APAL showed superior fatigue crack growth resistance, which may be attributed to the crack bridging effect imposed by the intact fibers in the crack wake. The magnitude of crack bridging was estimated quantitatively and determined by a new technique on basis of compliances of the 2024-T3 aluminum alloy and the APAL specimens. The crack growth rates of the APAL specimens were reduced significantly as comparison to the monolithic aluminum alloy and were not adequately correlated with the conventional stress intensity factor range (ΔK). It was found that the crack growth rate was successfully correlated with the effective stress intensity factor range ($\Delta K_{eff}=K_{br}-K_{cl}$) allowing for the crack closure and the crack bridging. The relation between da/dN and the ΔK_{eff} was plotted within a narrow scatter band regardless of kind of stress ratio (R=0.2, 0.5) and material (2024-T3 aluminum alloy, APAL 0 °/90° and APAL ±45°). The result equation was as follow : $da/dN=6.45\times10^{-7}(\Delta K_{eff})^{2.4}$.

Key Words : Hybrid Composite, Aramid/Epoxy Prepreg, Fatigue Crack Growth Behavior, Effective Stress Intensity Factor Range, Crack Bridging, Crack Closure

1. Introduction

The aluminum alloys have been the most popular as structural material in the aerospace and aircraft industries. The aluminum alloy has good charcteristics for high strength to weight ratio compared with other conventional metals. But, the aluminum alloy has low resistance for fatigue crack growth because of its brittleness for high strength. Therefore, many studies are required to make up for this weak point.

The advantages offered by advanced composite material over conventional alloys (for example ; aluminum alloy etc.) are widely recognized for structural applications requiring high strength and stiffness to weight. In addition, composite materials as a group have significantly greater property for fatigue loading than any other class of material known up to this time.

Currently, to high strength and stiffness combined with low density, advanced composites such as fiber-reinforced resin-matrix composites have good dimentional stability, corrosion resistance and good fatigue properties. However, resin-matrix composites employing thermosetting polymers generally exhibit brittle behavior. These, in turn, reduces the fracture toughness and damage tolerance of composite structure laminated exclusively with these laminate materials.

To circumvent the problems associated with traditional resin-matrix composites, hybrid composites consisting of two or more type materials at the lamina level are currently being introduced to

* Department of Mechanical Engineering, Dong-A University, Pusan, Korea
** Department of Mechanical Engineering, Dong-Eui Univ., Pusan, Korea
*** Han-Kuk Fiber Glass Co. Ltd., Kyungnam, Korea

the market (Davidson, 1991; Marissen, 1987; Ritchie, 1987, 1989, Volelesang, 1983, 1986). One of the emerging hybrid composites is ARALL laminate which was originally developed by Vogelesang(1983, 1986) and associates at Delft University and is currently marketed by the Aluminum Company of America. The ARALL laminates consist of alternating layers of thin aluminum alloy sheets bonded by a structural adhesive impregnated with high-strength unidirectional aramid fibers. It was primarily developed as a material with good damage tolerance properties.

Recent investigations (Davidson, 1991; Marissen, 1987; Ritchie, 1987, 1989; Volelesang, 1983, 1986) have shown that the ARALL laminates possess superior fatigue crack growth resistance to conventional high-strength aluminum alloys. These properties, together with high tensile strength along the fiber direction and low density, make the ARALL laminates attractive for aircraft structural applications where fatigue is an important design criterion. Advantages of the ARALL laminates over conventional monolithic aluminum alloy have been summarized by Bucci etc. (1988).

Most of the work on the ARALL has been directed towards determining its engineering properties under a variety of crack growth was performed by Marrissen(1984, 1987 and 1988) and Ritchie(1986, 1987 and 1989) etc.. Marissen's work, very comprehensive efforts to determine many characteristics of the ARALL, focused the mechanism part of the work mainly on delamination of the aluminum sheets near the crack line and behavior of the epoxy adhesive. The works of Ritchie etc. were much more concerned with the efforts of fiber bridging and closure, as measured using a back face strain gage. The focus of the effort was to determine the affects of both closure and bridging, on the stress intensity at the crack tip, and marked the first attempt to assess the factors locally. They found that crack growth rates generated under different conditions could be regulated well when an effective stress intensity factor (ΔK_{eff}) allowing for crack closure and bridging was used as the local crack driving force.

The performance of hibrid composites depends strongly on the type of reinforcing fibers (Koterazawa, 1993; Lin, 1991; Mall, 1987). Authors (Oh, 1993) have made many efforts for hibrid composites. In prior studies, the fatigue crack growth behavior of a hibrid composite (APAL ; Aramid Patched Aluminum Alloy) was found to be reduced extremely as comparison to that of the 2024-T3 aluminum alloy.

The APAL was a hybrid composite material, which is consisting of aluminum-alloy plate patched aramid cloth/epoxy laminate. Its crack growth rate was not properly correlated with the stress intensity factor range (ΔK). New prarameter needs to be developed to govern the crack growth rate. The effective stress intensity factor range (ΔK_{eff}) taking accounting of the crack closure and the crack bridging was introduced to solve the problem connected with the crack growth rate.

In this study, the objective was to describe a new experimental technique to measure quantitatively the magnitude of crack closure and crack bridging in order to determine the effective stress intensity factor (ΔK_{eff}). In addition, it was examined whether the parameter ΔK_{eff} was still effective for fiber orientation (0°/90°, 45°) and stress ratio (R=0.2, 0.5).

2. Experimental Procedures

2.1 Material

The composite studied in this study was a hybrid material designated APAL supplied HAN-KUK fiber glass Co. Ltd., Korea. As shown Fig. 1, The APAL was a laminate of

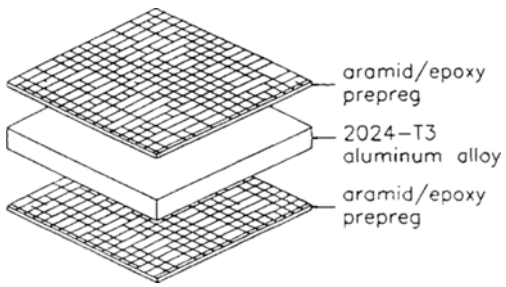

Fig. 1 Schematic illustration of APAL

Table 1 Chemical compositions of 2024-T3 aluminum alloy (wt.%)

Si	Fe	Cu	Mn	Mg	Cr	Zn	Ti	Al
0.11	0.23	4.46	0.58	1.44	0.04	0.03	0.02	Bal.

Table 2 Mechanical properties of 2024-T3 aluminum alloy

Yield strength (MPa)	Tensile stregth (MPa)	Elongation (%)	Hardness (Hv)
330	466	23.8	146.5

Table 3 Physical properties of aramid/epoxy prepreg (HK 285/RS 1222)

Volatile content	0.28%
Resin content	52.17%
Resin flow (at 0.35 MPa)	28.72%
Gel time (at 135±1℃)	4 min 48 sec

Table 4 Mechanical properties of aramid/epoxy laminate (HK 285/RS 1222)

Fiber pattern / Properties	Warp(0°) (MPa)	Fill(90°) (MPa)
Tensile strength	567.50	512.41
Tensile modulus	30000.35	31000.04
Compression strength	224.14	227.59
Compression modulus	29000.66	29000.66
Flexural strength	513.79	510.35
Inter laminar shear strength	63.45	-

2024-T3 aluminum alloy plate sandwitched with two sheets of aramid fiber/epoxy prepregs. The aluminum alloy plate was 6.5 mm thick and the each aramid fiber/epoxy prepreg (HK #285/RS 1222) was about 0.25 thick. The aramid/epoxy prepreg was a sheet of Kevlar aramid fibers embedded in epoxy resin. Tables 1 and 2 show the chemical compositions and the mechanical properties of the 2024-T3 aluminum alloy. Tables 3 and 4 show the physical properties and the mechanical properties of the aramid/epoxy prepreg. Two plies of the aramid/epoxy prepreg sheets were cured at 127℃ to double sides of a surface treated aluminum alloy plate. The APAL specimens used were two kinds with different fiber orientation of 0°/90° and ±45° for crack direction, where the aluminum alloy specimen plate was manufactured for L-T orientation, as shown Fig. 2.

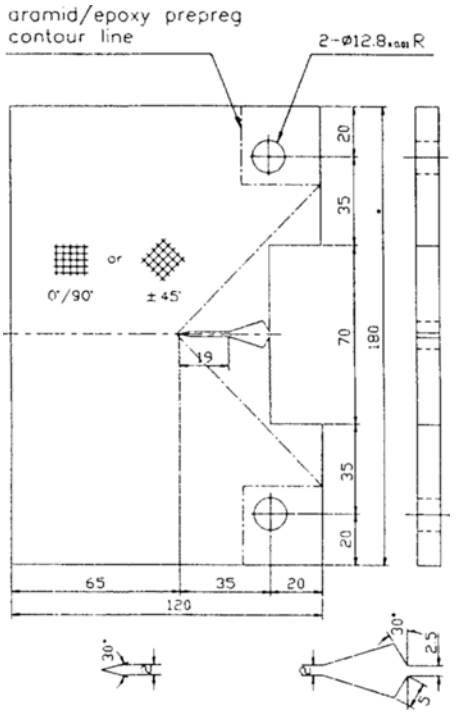

Fig. 2 Shape and dimension of specimen for fatigue test

2.2 Fatigue test

Fatigue crack growth tests were performed using CT specimens of 2024-T3 aluminum alloy and APALs. All tests were carried out using a servohydraulic testing machine (MTS model 810, 10 tonf) with load control mode, two stress ratios $R=0.2$, 0.5, waveform sinusoidal and frequency 15 Hz.

The fatigue crack length was monitored by the compliance method, and was measured by a travelling microscope and a beach mark method.

The crack closure was analyzed using a back-face strain gage mounted on the aluminum plate and a COD gage sticked to crack mouth.

3. Result and Discussion

3.1 Measurement of crack length

Figure 3 shows the relation between the compliance crack length (a_c) by compliance method and the measured true crack length (a_M). The compliance crack length was determined on basis of the compliance value using the crack opening displacement (COD) at loading line. The measured crack length was the value measured on surface by a travelling microscope in case of the 2024-T3 aluminum alloy specimen, and the value determined by beach mark method in case of the APAL specimen. The compliance crack lengths (a_c) were nearly equal to the measured crack lengths (a_M) for the both stress ratios ($R=0.2$, 0.5) regardless of stress ratio in the aluminum alloy and the APAL specimens. In case of the aluminum alloy, the compliance crack lengths were almost identical to the measured crack lengths. In case of the APAL, the compliance crack lengths were smaller than the measured crack length. The magnitudes of differences were larger in the APAL 0°/90°than in the APAL ±45°.

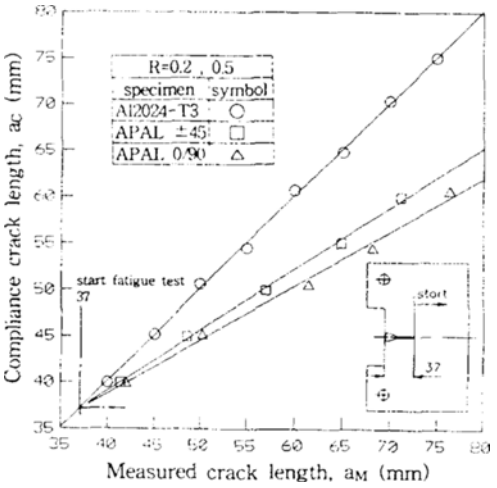

Fig. 3 Comparison of compliance crack length and measured crack length by beach mark method

3.2 Fatigue crack growth behavior

Figure 4 shows the relation between fatigue crack growth rate (da/dN) and stress intensity factor range (ΔK) at two stress ratios ($R=0.2$, 0.5) for the aluminum alloy. The fatigue crack growth rate was similar in both stress ratios ($R=0.2$, 0.5) and was plotted on a line with little scattering, which implied that the crack growth rate was not effected by stress ratio. It have been reported that the effect of stress ratio on fatigue crack growth rate is resulted from the crack closure (Hudson, 1969; Newman, 1984; Allison, 1988; Omer, 1990). This behavior being independent of stress ratio indicated that the crack closure was not developed in this test condition. In actual, the crack cloure was measured using a clip gage at loading line and a back face strain gage, but it was scarcely detected in both methods in this experiment. Accordingly, it could be considered that the crack closure was not originated in this test condition.

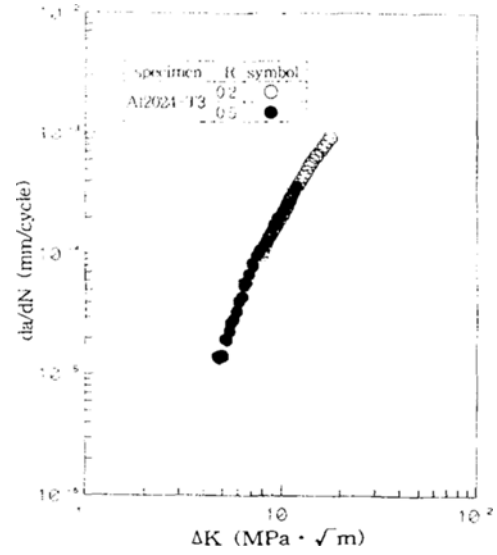

Fig. 4 Relation between fatigue crack growth rate and stress intensity factor range for 2024-T3 aluminum alloy

As a result, the fatigue crack growth rate, in the aluminum alloy, was expressed as a function of stress intensity factor range. This figure thus indicated that stress intensity factor range (ΔK) was good parameter for the fatigue crack growth rate in the aluminum alloy.

Figures 5 and 6 show the relation between fatigue crack growth rate (da/dN) and stress intensity factor range (ΔK) at stress ratios of $R=$

0.2, 0.5 in the APAL 0°/90° and the APAL ±45°, compared with the aluminum alloy. The fatigue crack growth behavior of the APAL was great different from that of the aluminum alloy. The fatigue crack growth rate in the APAL was remarkably slower than that in the aluminum alloy and the amount of difference in fatigue crack growth rate got larger as the stress intensity factor range level was increased. Its reduction is very very significant. It may be said that the APAL possesses splendid fatigue crack growth resistance compared with the aluminum alloy.

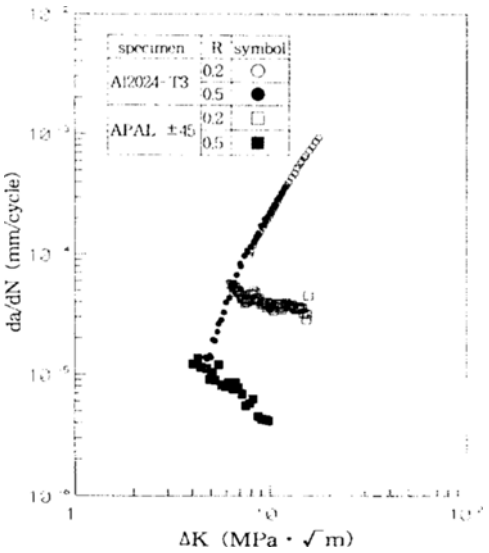

Fig. 5 Relation between fatigue crack growth rate and stress intensity factor range for APAL ±45°

The fatigue crack growth behavior of the APAL was peculiar for stress intensity factor range (ΔK) and stress ratio, compared to the aluminum alloy. Though fatigue crack growth rate must be increased as ΔK level was increased, here cases of the APAL were found to be decreased conversely. In addition, the fatigue crack growth rate generally get fast as stress ratio goes high, but the fatigue crack growth rate for higher stress ratio $R = 0.5$ was very slower than that for $R = 0.2$, so here a contrary behavior was shown for the stress ratio.

All results of the constant-amplitude fatigue crack growth test, in the form of growth rates, as a function of stress intensity factor range are shown in Fig. 7 to compare growth rates for the APAL 0°/90° and the APAL ±45°. The reduction in growth rates was remarkably for two kinds of the APAL compared with the 2024-T3 aluminum alloy. In addition, it was obvious that

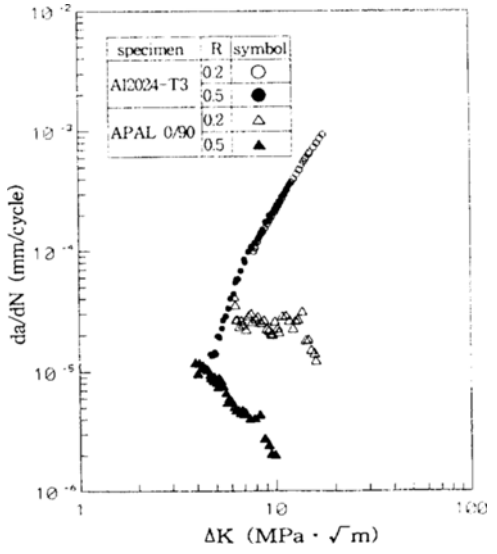

Fig. 6 Relation between fatigue crack growth rate and stress intensity factor range for APAL 0°/90°

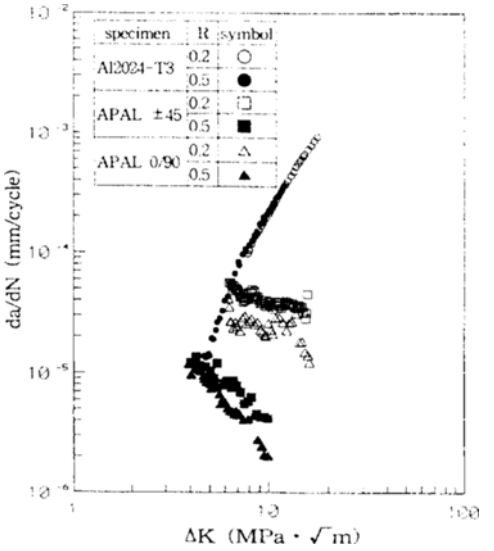

Fig. 7 Relation between fatigue crack growth rate and stress intensity factor range for all test conditions

the fatigue crack growth rate of the APAL appeared different from fiber orientation. The APAL 0°/90°which fiber orientation was 0°and 90 to crack direction had greater fatigue crack growth resistance than the APAL ±45°which fiber orientation was ±45°. This is resulted from that the APAL 0°/90° have more larger stiffness than the APAL ±45°.

3.3 Effect of fiber bridging

The reason why the fatigue crack growth rate of the APAL was reduced compared with the 2024-T3 aluminum alloy was that fatigue crack growth was hindered by the aramid/epoxy laminate adhered to double surfaces. In specimens of the APAL being finished fatigue test, fatigue crack was propagated on the aluminum alloy. However, on the aramid/epoxy prepreg, fatigue crack was hardly made and propagated. When fatigue crack was propagated on the aluminum alloy in specimen of the APAL, the aramid/epoxy laminate was debonded from the aluminum alloy in the wake of the crack tip, and the shape of the debonded area was formed into triangular shape. Exceedingly partial fibers were damaged on the debonded area and most fibers remained intact.

Marissen(1984) have reported that Aramid fiber reinforced aluminum alloy laminates (ARALL) similar to the APAL derives superior crack growth resitance by promoting extensive crack bridging in the wake of the crack tip. The individual fibers remaining intact span the crack in the wake of the crack tip. Thus, similar to behavior in certain ceramic-matrix composites (Marshall, 1987) the fibers act as bridges to restain crack opening, thereby reduce the effective crack driving force actually experienced at the crack tip. Crack bridging is an example of crack-tip shielding, where toughness is enhanced, or more generally crack advance is impeded, not by increasing the intrinsic microstructural resistance but by mechanisms which act to lower the local near-tip driving force (Ritchie, 1987, 1989).

According to Ritchie(1987, 1989) et. al., the crack driving force should be better represented by the effective stress intensity factor range (ΔK_{eff}), which embodies the effect of both crack bridging as well as crack closure.

3.3.1 Principle

The principle of the measurement technique for the shielding by crack bridging and closure was illustrated schematically in Fig. 8. Shielding is assumed to affect the applied crack driving force, $\Delta K = K_{max} - K_{min}$, in two ways. One is crack closure (i.e. physical contact between crack surface) and the other is crack bridging, which primarily decreases the effective K_{max}. Accordingly, the effective stress intensity experienced at the tip may be defined as : $\Delta K_{eff} = K_{br} - K_{cl}$, where K_{br} is the effective K_{max} (corrected for crack bridging) and K_{cl} is the effective K_{min} (corrected for crack closure). Experimental techniques to measure each parameter are described below.

3.3.2 Crack closure

In aluminum alloys at low ΔK level, the principal source of crack closure arises from wedging of

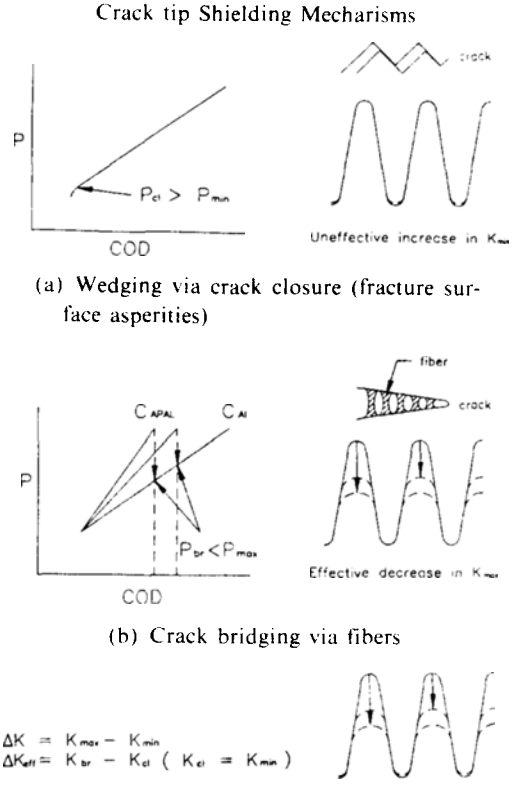

Fig. 8 Schematic illustration of the primary crack-tip shielding mechanism in APAL (crack bridging and crack closure)

crack surface by fracture-surface asperites (roughness-induced closure), aided by that induced by cyclic plasticity in the wake of the crack tip. Accordingly, the closure stress intensity K_{cl} is generally measured at first contact point of the crack surface during an unloading cycle. In the present study, this crack closure was measured by monitoring the elastic unloading compliance derived from the clip gage at loading line and the back-face strain gage. Specifically, the data acquisition and control system were programmed to determine the K_{cl} value in real time in terms of the highest load where the elastic unloading compliance curve deviated from linearity.

Using such procedures, however, closure level was found to be small negligibly in this condition of test for the 2024-T3 aluminum alloy and the APAL (Fig. 8(a)). The reason of small crack closure was thought that the fatigue crack growth rate level was too high in this condition of test.

In fact, the crack closure was clearly of secondary importance to the crack bridging in governing the value of ΔK_{eff}.

3.3.3 Crack bridging

The effect of the crack bridging on the effective K_{max} value was estimated using a new technique which combined determination of the actual length, using calibration chart of Fig. 3, with measurement by the compliance of the bridged crack, using clip gage at loading line. For each cycle, on the elastic compliance curve of the actual crack opening displacement (COD) vs. load (P) determined in the APAL specimen ; the slope of this curve (ignoring non-linearities due to closure at very low loads) represented the compliance of the bridged crack. In addition, the true length of the crack was estimated using the experimentally verified compliance calibration in Fig. 3. On elastic compliance curve by the COD of the aluminum alloy at the crack length corresponding to the true crack length of the APAL specimen vs. load (P) in aluminum alloy ; the slope of this curve represented the compliance of the unbridged crack. As illustrated in Fig. 8, the slopes of these two curves were different. The curve, derived from clip gage measurement, was steeper (implying a smaller effective crack size) because the compliance is reduced by the fiber bridging ; and the curve, derived from the true crack length, is insensitive to the bridging effect.

Thus, at maximum load, the COD determined by the clip gage measurement (bridged) could be seen to be less than that predicted from the true (unbridged) crack length, because of the restraint on crack opening by the fibers. On this basis, the reduction in effective K_{max} due to fiber bridging could be estimated by comparing these two curves.

As shown in Fig. 8(b), the P at maxium COD in the APAL got down largely than that of the aluminum alloy at the maxium COD of the APAL ; the reduction is essentially the load carried by the bridging fibers. Accordingly, the value of the Pbr can be used to compute magnitude of K_{br} as the effective maximum stress intensity.

Figure 9 shows the relation between the COD $_{max}$ at loading line and the true (unbridged) crack length in all test specimens in order to determine bridging quantitatively. As shown in Fig. 9, the COD_{max} for the APAL specimens is smaller than that for the 2024-T3 aluminum alloy specimen at a given (true) crack length, because of the effect of bridging. In the APAL 0°/90°is smaller than that in the APAL ±45°. As to stress ratio, the COD_{max} for $R=0.2$ and $R=0.5$ are identical in case of the aluminum alloy specimen, but, in case of the

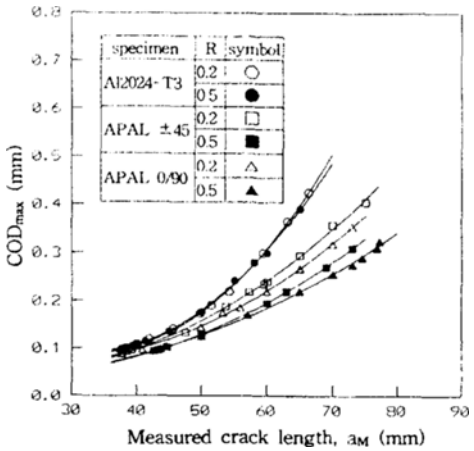

Fig. 9 Relation between COD_{max} and measured crack length in order to estimate crack bridging

APAL specimen, the COD_{max} for $R=0.2$ is larger than that for $R=0.5$.

In the APAL specimens, the intact fibers around the wake of crack tip restrained the crack opening and thus carried some portion of total load, that is, the bridging phenomenon was developed. The amount of load that the fiber carried did not exercised no influence on the crack growth. The effective load for the crack growth was the value after subtracting the load for the fibers from the total load. The magnitude of load that the fibers carried was in proportion to the reduction of the COD_{max} of the APAL specimens in comparison with the COD_{max} of the aluminum alloy. Accordingly, the effective load ($\Delta P_{eff}=P_{br}-P_{cl}$) could be determined quantitatively on basis of Fig. 9 and ΔK_{eff} was calculated corresponding to the P_{eff}.

Figure 10 shows the value of the $\Delta K_{eff}/\Delta K$ determined at a given true carck length, using the result of Fig. 9. In actual, the effective stress intensity factor range (ΔK_{eff}) is reduced considerably in comparison with the stress intensity factor range (ΔK) and the amount of reduction grew large as the crack length was increasing. The effect of crack bridging on the APAL specimen was found to be great in K_{max} values during the fatigue cycle. With such procedure, the result of Fig. 8 for crack growth at constant ΔK was replotted in terms of ΔK_{eff}, as Fig. 11. The fatigue crack growth rate was then correlated with the effective stress intensity factor range, ΔK_{eff}, for all specimens of test. As a result, good result was achieved for all the test conditions. The relation between da/dN and ΔK_{eff}, in the APAL specimens, was found to be plotted within a narrow scatter band for both the APAL specimens and the stress ratios. Moreover, the test points for the 2024-T3 aluminum alloy also were distributed within the same scatter band.

Therefore, once the allowance is made for both closure and bridging in the computation of the appropriate crack driving force , crack growth behavior is no longer dependent upon stress ratio and material, and is a unique function of only ΔK_{eff}. Hence, it can be concluded that ΔK_{eff} is the governing parameter regardless of kind of

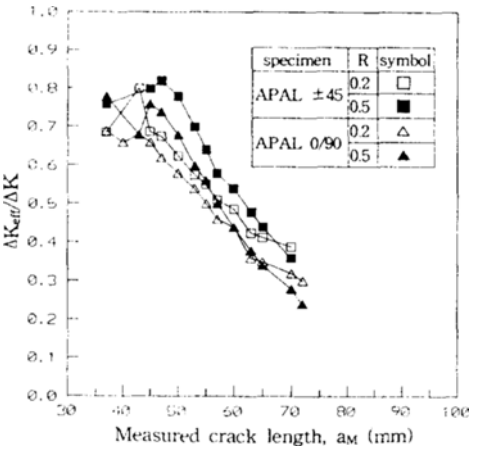

Fig. 10 Relation between $\Delta K_{eff}/\Delta K$ and measured crack length in order to estimate crack bridging

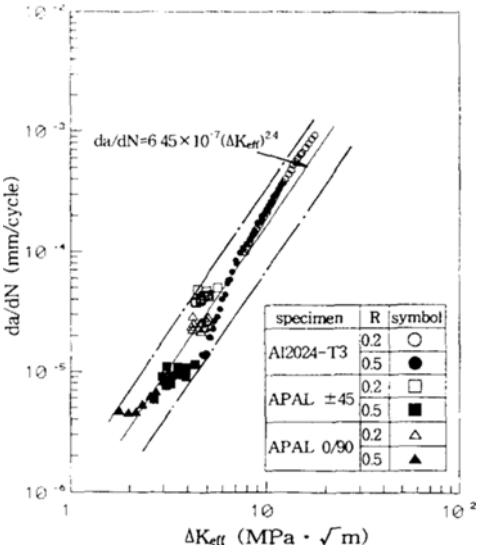

Fig. 11 Relation between fatigue crack growth rate and effective stress intensity factor range ($\Delta K_{eff}=K_{br}-K_{cl}$) for all test conditions

material and stress ratio. Based on this result, a power-law relation as Paris'(1963) equation can be expressed as the following,

$$da/dN=6.45\times10^{-7}(\Delta K_{eff})^{2.4} \quad (1)$$

4. Conclusion

The fatigue crack growth test has been carried

out at stress ratio $R=0.2$, 0.5 using 2024-T3 aluminum alloy, the APAL 0°/90° and the APAL ±45° (Aramid Patched Aluminum Alloy), a driving parameter for crack growth rate in all the test conditions. The results was as follows :

(1) The APAL derived excellently superior crack growth resistance to 2024-T3 aluminum alloy, thus the fatigue crack growth rate of the APAL was reduced extremely compared with that of the aluminum alloy. The conventional parameter, stress intensity factor range (ΔK), was impossible to correlate with the fatigue crack growth rate in the APAL specimens.

(2) In the APAL specimens, the effectiveness of the reduction of the crack growth rate was found to be dependent on the crack bridging by the fibers. The crack bridging was estimated quantitatively by a new technique on basis of the compliances at loading line of 2024-T3 aluminum alloy and the APAL specimens, and the ΔK_{eff} ($\Delta K_{eff}=K_{br}-K_{cl}$) was determined allowing the crack bridging.

(3) The fatigue crack growth rate (da/dN) was regulated as a function of ΔK_{eff}. It was found that the crack growth rate was successfully correlated with the ΔK_{eff} and so the reduction of the crack growth rate in the APAL was explained using this parameter. The relation between da/dN and ΔK_{eff} was plotted within a narrow scatter band regarless of kind of the stress ratios ($R=0.2$, 0.5) and the materials (2024-T3 aluminum alloy, APAL 0°/90° and, APAL ±45°). The result equation was as follow : $da/dN=6.45\times10^{-7}(\Delta K_{eff})^{2.4}$.

References

Allison, J. E., 1988, "On the Measurement of Crack Closure During Fatigue Crack Growth," *in Fracture Mechanics 18th Symp. ASTM*, Philadelphia, PA, pp. 913~933.

Bucci, R. T., Muelle, I. N., Volelesang, L. B. and Gunnink, J. W., 1988, "ARALL Laminates Properties and Design Update," *Proc. 33rd Int. SAMPE Symp.*, 7-10 March, pp. 1237~1248.

Davidson, D. L. and Austin, L. K., 1991, "Fatigue Crack Growth Through ARALL-4 at Ambient Temperature," *Fatigue Fract. Engng. Mateer. Struct.* Vol. 14, No. 10, pp. 939~951.

Hudson, C. M. and Scardina, J. T., 1969, "Effect of Stress Ratio on Fatigue Crack Growth in 7075-T3 Aluminum Alloy Sheet," *Eng. Fract. Mech.*, Vol. 1, pp. 429~446.

Koterazawa, R., Nose, M. et al., 1993, "Fatigue Crack Growth and Fatigue Danmage Development in Fiber Reinforced Composites Under Variable Amplitude Stresses," *J. Soc. Mat. Sci. Japan*, Vol. 42, No. 472, pp. 46~51.

Lin, C. T., Kao, P. W. and Lang, F. S., 1991, "Fatigue Behaviour of Carbon Fiber-Reinfoced Aluminum Laminates," *Composites*, Vol. 22, No. 2, pp. 135~141.

Mall, S., Ramamurthy, G. and Rezaizdeh, M. A., 1987, "Stress Ratio Effect on Cyclic Debonding in Adhesively Bonded Composite Joints," *Composite Structures*, Vol. 8, pp. 31~45.

Marissen, R., 1984, "Flight Simulation Behavior of Aramid Reinforced Aluminum Laminates(ARALL)," *Eng. Fract. Mech.*, Vol. 19, pp. 261~277.

Marissen, R., 1987, "Fatigue Mechanisms in ARALL, a Fatigue Resistant Hybrid Aluminum Aramid Composite Material," *In Fatigue 87*, pp. 1271-1279, EMAS Ltd, Warlery, U.K.

Marissen, R, 1988, "Fatigue Crack Growth in ARALL," Thesis, Technical Univ. of Delft. The Netherlands. Published in English as DFVLR-F 88-56.

Newman, J. C., et al., 1984, "A Crack Closure Model for Predicting Fatigue Crack Growth under Aircraft Spectrum Loading," *ASTM STP 748*, pp. 53~84.

Oh, S. O., Yoon, H. K. and Park, W. J. et al., 1993, "Fatigue Crack Growth Behavior in 2024-T3 Aluminum Alloy Plate with Aramid Fiber Reinforced(APAL) (I)," *Proceeding of KSME*, Oct, pp. 17~21.

Oh, S. O., Yoon, H. K. and Park, W. J. et al., 1993, "Fatigue Crack Growth Behavior in 2024-T3 Aluminum Alloy Plate with Aramid Fiber Reinforced(APAL)(II)," *Proceeding of KCORE*, Oct., pp. 177~182.

Omer, G. B. and Metin Harun, 1990, "Effect of Stress Ratio on the Rate of Growth of Fatigue

Cracks in 1100 Al-Alloy," *Engng. Fract. Mech.*, Vol. 37, No. 6, pp. 1203~1206.

Paris, P. C. and Erdogan, F., 1963, "A Critical Analysis of Crack Propagation Laws," *Trans. ASME, J. of Basic Eng. 85*, pp. 528~534.

Ritchie, R. O. and Yu, W., 1986, "Short Crack Effects in Fatigue," *TMS-AIME, Warrendale, PA*, pp. 7~198.

Ritchie, R. O., 1987, "Crack Tip Shielding in Fatigue, in Mechanical Behavior of Materials-V," *Proc. 5th Int. ICM Conf.*, Vol. 3, Pergamon Press, Oxford, U.K.

Ritchie, R. O., 1987, "Crack Tip Shielding in Fatigue, in Mechanical Behavior of Materials-V," *Proc. 5th Int. Conf.* Vol. 3, Pergamon Press, Oxford, U.K.

Ritchie, R. O, Yu, W. and Bucci, R. J., 1989, "Fatigue Crack Propagation in ARALL Laminates : Measurement of the Effect of Crack-tip Shielding from Crack Bridging," *Engineering Fracture Mechanics*, Vol. 32, No. 3, pp. 361~377.

Vogelesang, L. B. and Gunnink, J. W., 1983, "ARALL a Material for the next Generation of Aircraft," *A State of Aat. Report LR-400*, Delft Univ. of Technology, Dept. of Aerospace Engineering, August.

Vogelesang, L. B. and Gunnick, J. W., 1986, "ARALL, a Materials Challenge for the Next Generation of Aircraft," Mater. Design, 7, 2.